

Iron oxides stimulate sulfate-driven anaerobic methane oxidation in seeps

Orit Sivan^{a,1}, Gilad Antler^b, Alexandra V. Turchyn^b, Jeffrey J. Marlow^c, and Victoria J. Orphan^c

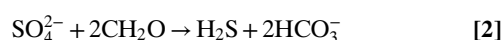
^aDepartment of Geological and Environmental Sciences, Ben Gurion University of the Negev, Beer-Sheva 84105, Israel; ^bDepartment of Earth Sciences, University of Cambridge, Cambridge CB2 3EQ, United Kingdom; and ^cDivision of Geological and Planetary Sciences, California Institute of Technology, Pasadena, CA 91125

Edited by Mark H. Thiemens, University of California, San Diego, La Jolla, CA, and approved August 28, 2014 (received for review June 30, 2014)

Seep sediments are dominated by intensive microbial sulfate reduction coupled to the anaerobic oxidation of methane (AOM). Through geochemical measurements of incubation experiments with methane seep sediments collected from Hydrate Ridge, we provide insight into the role of iron oxides in sulfate-driven AOM. Seep sediments incubated with ¹³C-labeled methane showed co-occurring sulfate reduction, AOM, and methanogenesis. The isotope fractionation factors for sulfur and oxygen isotopes in sulfate were about 40‰ and 22‰, respectively, reinforcing the difference between microbial sulfate reduction in methane seeps versus other sedimentary environments (for example, sulfur isotope fractionation above 60‰ in sulfate reduction coupled to organic carbon oxidation or in diffusive sedimentary sulfate–methane transition zone). The addition of hematite to these microcosm experiments resulted in significant microbial iron reduction as well as enhancing sulfate-driven AOM. The magnitude of the isotope fractionation of sulfur and oxygen isotopes in sulfate from these incubations was lowered by about 50%, indicating the involvement of iron oxides during sulfate reduction in methane seeps. The similar relative change between the oxygen versus sulfur isotopes of sulfate in all experiments (with and without hematite addition) suggests that oxidized forms of iron, naturally present in the sediment incubations, were involved in sulfate reduction, with hematite addition increasing the sulfate recycling or the activity of sulfur-cycling microorganisms by about 40%. These results highlight a role for natural iron oxides during bacterial sulfate reduction in methane seeps not only as nutrient but also as stimulator of sulfur recycling.

redox | anaerobic respiration | deep-sea | methanotrophy | ANME archaea

Microbial dissimilatory processes generate energy through the decomposition of substrates, whereas assimilatory processes use substrates for intracellular biosynthesis of macromolecules. The most known and energetically favorable dissimilatory process is the oxidation of organic carbon coupled to oxygen as terminal electron acceptor (Eq. 1). In sediments with a high supply of organic carbon, oxygen can be depleted within the upper few millimeters, leading to anoxic conditions deeper in the sediment column. Under these conditions, microbial dissimilatory processes are coupled to the reduction of a series of other terminal electron acceptors besides oxygen (1). The largest free-energy yields are associated with nitrate reduction (denitrification), followed by manganese and iron oxide reduction, and then sulfate reduction. Due to the high concentration of sulfate in the ocean, dissimilatory bacterial sulfate reduction (Eq. 2) is responsible for the majority of organic matter oxidation in marine sediments (2). Below the depth of sulfate depletion, traditionally the only presumed process is methanogenesis (methane production), where its main pathways are fermentation of organic matter, mainly acetate (Eq. 3), or the reduction of carbon dioxide with hydrogen as substrate (Eq. 4) (3):



When methane that has been produced deep in sediments diffuses into contact with an available electron acceptor, it can be oxidized (methanotrophy). Methanotrophy is the main process that prevents the escape of methane produced within marine and fresh water sediments into the atmosphere. In fresh water systems, methanotrophic bacteria are responsible for oxidizing methane to dissolved inorganic carbon (DIC) typically using oxygen as an electron acceptor (4, 5). In marine sediments, however, where oxygen diffusion is limited, anaerobic oxidation of methane (AOM) coupled to sulfate reduction [e.g., refs. 6 and 7 (Eq. 5)] has been shown to consume up to 90% of the methane produced within the subseafloor environment (8). Often, when methane is present, the majority of sulfate available in marine pore fluids is reduced through sulfate-driven AOM (9–13):



Other electron acceptors such as nitrate and oxides of iron and manganese, could also oxidize methane anaerobically and provide a greater free-energy yield than sulfate-coupled methane oxidation (14). Indeed, Beal et al. (15) showed the potential for iron- and manganese-driven AOM in microcosm experiments with methane seep sediments from Eel River Basin and Hydrate Ridge, and iron-driven AOM has been interpreted from modeling geochemical profiles in deep-sea sediments (13, 16).

Significance

Anaerobic oxidation of methane (AOM) coupled to sulfate reduction has been shown to consume up to 90% of the greenhouse gas methane produced within the subseafloor environment; however, the mechanism of this process has remained enigmatic. Here, we provide geochemical evidence based on sulfur, oxygen, and carbon isotopes for the involvement of iron oxides in sulfate-driven AOM in methane seeps. Our results suggest that, beyond the function of iron as nutrient, the presence of iron oxides stimulates sulfate-driven AOM to a greater extent than in sediments with low concentrations of iron oxides. The isotope analyses further indicate that sulfate reduction in methane seep habitats differs than sulfate reduction in diffusive profiles in and above the sulfate–methane transition zone.

Author contributions: O.S. and V.J.O. designed research; O.S., G.A., and J.J.M. performed research; O.S., G.A., A.V.T., J.J.M., and V.J.O. analyzed data; and O.S., G.A., A.V.T., J.J.M., and V.J.O. wrote the paper.

The authors declare no conflict of interest.

This article is a PNAS Direct Submission.

¹To whom correspondence should be addressed. Email: oritsi@bgu.ac.il.

This article contains supporting information online at www.pnas.org/lookup/suppl/doi:10.1073/pnas.1412269111/-DCSupplemental.

AOM has been shown to occur in nonmarine sediments via denitrification (17–21) and iron reduction (22, 23). However, all geochemical and microbiological studies point to sulfate-driven AOM as the dominant sink for methane in marine sediments.

Sulfate-driven AOM is understood to involve microbial consortia of archaea and bacteria affiliated with archaeal methanotrophs (“methane oxidizers”) and sulfate-reducing bacteria (11, 24). A common view is that anaerobic methanotrophic archaea (ANME) oxidize methane, while the sulfate-reducing syntrophic partner scavenges the resulting reducing equivalents to reduce sulfate to sulfide (7, 25, 26). Recently, however, cultured AOM enrichments from seeps were reported to be capable of direct coupling of methane oxidation and sulfate reduction by the ANME-2 archaea, with the passage of zero valent sulfur to a disproportionating bacterial partner, capable of simultaneously oxidizing and reducing this substrate to sulfate and sulfide in a ratio of 1:7, respectively (27). Whether this “single organism mechanism” for sulfate-driven AOM is widespread in the natural environment, or whether there is a diversity of mechanisms for sulfate-driven AOM, remains enigmatic.

Carbon isotopes provide a good constraint on the depth distribution and location of methanogenesis and methanotrophy because of the carbon isotope fractionation associated with these processes (e.g., refs. 28 and 29). During methanogenesis, ^{12}C is strongly partitioned into methane; the $\delta^{13}\text{C}$ of the methane produced can be between -50‰ to -110‰ . In parallel, the residual DIC pool in methanogenic zones becomes highly enriched in ^{13}C , occasionally by as much as 50‰ to 70‰ (e.g., ref. 28). Oxidizing this methane on the other hand, results in ^{13}C -depleted DIC and slightly heavier $\delta^{13}\text{C}$ values of the residual methane, caused by a fractionation of 0‰ to 10‰ during methane oxidation and the initial negative $\delta^{13}\text{C}$ value of the methane itself (30, 31).

The sulfur and oxygen isotopes in dissolved sulfate ($\delta^{34}\text{S}_{\text{SO}_4}$ and $\delta^{18}\text{O}_{\text{SO}_4}$) may also be a diagnostic tool for tracking the pathways of sulfate reduction by methane or other organic compounds. Sulfur isotope fractionation during dissimilatory bacterial sulfate reduction, which partitions ^{32}S into the sulfide, leaving ^{34}S behind in the residual sulfate, can be as high as 72‰ (32–35). As sulfate is reduced to sulfide via intracellular intermediates (34, 36–40), the magnitude of this sulfur isotope fractionation depends upon the isotope partitioning at each of the intercellular steps and on the ratio between the backward and forward sulfur fluxes within the bacterial cells (34, 36).

Oxygen isotopes in sulfate, however, have been shown to be strongly influenced by the oxygen isotope composition of water in which the bacteria are grown (41–45). The consensus is that, within the cell, sulfur compounds, such as sulfite, and water exchange oxygen atoms; some of these isotopically equilibrated molecules return to the extracellular sulfate pool. As all of the intercellular steps are considered to be reversible (e.g., refs. 34, 36, 46, and 47), water–oxygen is also incorporated during the oxidation of these sulfur intermediates back to sulfate (41–43, 48–51).

Therefore, both oxygen and sulfur isotopes in the residual sulfate during dissimilatory sulfate reduction are affected by the changes in the intracellular fluxes of sulfur species. However, these isotopes in the residual sulfate are affected in different ways, and thus the change of one isotope vs. the other helps uniquely solve for the relative change in the flux of each intracellular step as sulfate is being reduced (42, 43, 50). The sulfur and oxygen isotope composition of residual sulfate has been used to explore the mechanism of traditional (organoclastic) sulfate reduction both in pure culture (e.g., refs. 44, 45, and 52) and in the natural environment (e.g., refs. 12, 49, 50, and 53–55). The coupled isotope approach has been used specifically to study sulfate-driven AOM recently in estuaries (56). In the work of Antler et al. (56), it was shown that the oxygen and sulfur isotopes in the residual sulfate in the pore fluids are linearly

correlated during sulfate-driven AOM, whereas during organoclastic bacterial sulfate reduction, the isotopes exhibit a concaved curve relationship.

Although iron and manganese oxides should be reduced before the onset of dissimilatory bacterial sulfate reduction in the natural environment from thermodynamic considerations, due to their low solubility, they may not be completely reduced through dissimilatory respiration when sulfate reduction starts (e.g., ref. 22). These lower reactivity manganese and iron oxides therefore may still be present during the lower-energy yielding anaerobic processes such as sulfate reduction, methanotrophy, and methanogenesis. Indeed, iron oxides have been shown to serve as electron acceptors for methane oxidation even in the sulfate “zone” (15, 16, 22, 57), although the mechanism of this coupling remains enigmatic. In the context of deep-sea methane seep ecosystems, earlier work by Beal et al. (15) demonstrated stimulation of AOM by the addition of iron and manganese oxides in sediment incubation experiments. In that work, however, the nature of the coupling between methane oxidation and metal oxides was not ascertained, and the multiple links between the sediment sulfur, iron, and methane cycles are equivocal.

Here, we conducted microcosm experiments with sediments collected from Hydrate Ridge South (Fig. S1) and used synergistic combinations of isotope analyses ($\delta^{34}\text{S}_{\text{SO}_4}$, $\delta^{18}\text{O}_{\text{SO}_4}$, and $\delta^{13}\text{C}_{\text{DIC}}$) to aid in assessing whether methane oxidation is directly coupled to the respiration of iron oxides or whether stimulation in methanotrophy is a result of the coupling between iron and sulfate. We provide compelling evidence for the stimulation of AOM in seep sediments through the coupling between iron and sulfate, and propose a mechanism for iron involvement in sulfate-driven AOM. Using microcosm experiments with seep sediments dominated by sulfate-driven AOM and amended with hematite and ^{13}C -labeled methane and glucose, we are able to demonstrate the role of iron in sulfate-driven AOM. Hematite is a less reactive form of iron oxide than, for example, amorphous iron (58), and it was used to prevent the microbial populations from “switching” completely to the more energetically favorable process of iron reduction.

Results

The incubation experiment was performed over the course of several months because of the long doubling time of the microorganisms involved in sulfate-coupled methane oxidation (~3 mo; refs. 59–61). Fig. 1 presents the results of the concentration of ferrous iron, methane, sulfate, and DIC over the course of the 6-mo experiment. Hematite was added to the bottles with the addition of $^{13}\text{CH}_4$ (Table S1), and measurements were performed on the day of hematite addition and approximately every 30 d thereafter.

Ferrous iron concentrations show that the addition of 12.5 mM hematite resulted in intensive biological reduction of ferric iron to ferrous iron of about 150 μM after 30 d (and no increase in the killed control) (Fig. 1A). After about 80 d, ferrous iron concentrations started to decrease, accompanied by the appearance of black particles that were likely iron sulfides (Fig. S2). Thus, iron reduction might continue past this point of the experiment but is masked by this iron–mineral precipitation. The seep sediments used in these experiments were selected because they (or adjacent cores) were shown to have active net anaerobic oxidation of methane; however, the methane concentration results from our experiments suggest some additional, if slight, production of methane of about 100 μM in all nonkilled bottles (Fig. 1B), maybe due to back reaction of AOM process, as suggested by Holler et al. (47) and Yoshinaga et al. (62). It seems also that methane was released by diffusion from the slurries to the headspace in all bottles, explaining the increase in methane concentration after the initial first day measurement also in the killed bottles (63). Sulfate concentrations (Fig. 1C) show a significant decrease with time from initial concentrations of

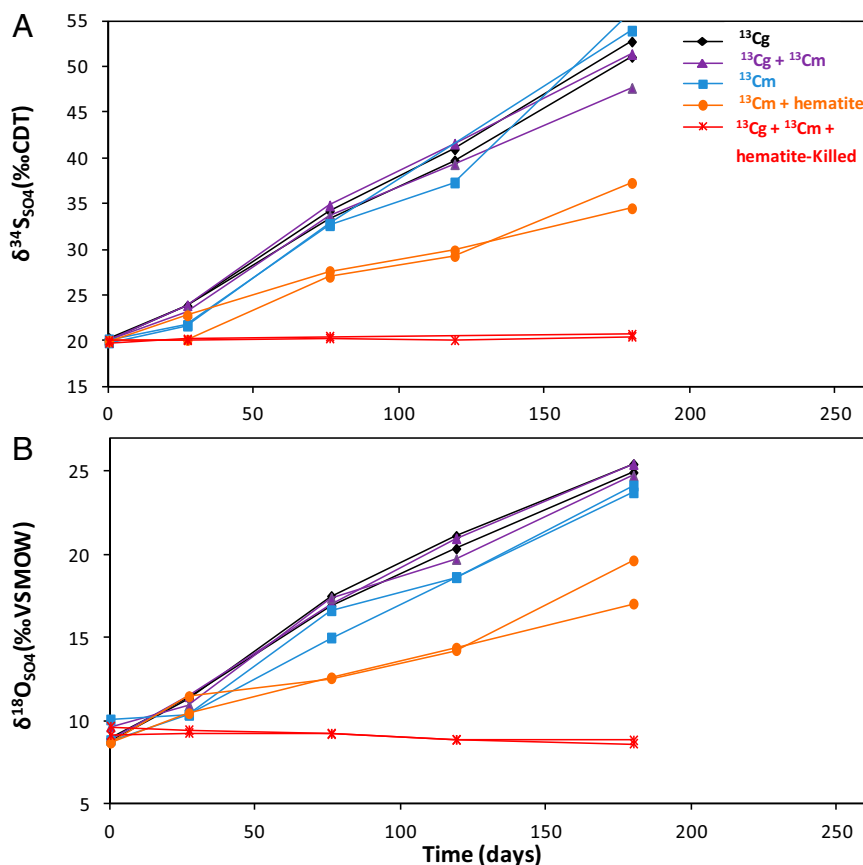


Fig. 3. The isotopic composition in sulfate of sulfur ($\delta^{34}\text{S}_{\text{SO}_4}$; **A**) and oxygen ($\delta^{18}\text{O}_{\text{SO}_4}$; **B**) over time with the different treatments as a result of the initial labeling with ^{13}C -glucose (g) and ^{13}C -methane (m). The error is smaller than the symbol. Note that the measured value of $\delta^{18}\text{O}$ of the water was $-0.7 \pm 0.05\text{‰}$.

$\delta^{13}\text{C}_{\text{DIC}}$. Our multiple isotope analysis can be used to distinguish between the possibilities of direct iron-driven AOM and this indirect iron stimulation of sulfate-driven AOM, and more directly determine the involvement of iron in AOM by microorganisms in deep-sea methane seep sediments.

Oxygen and sulfur isotopes in the residual sulfate during bacterial sulfate reduction can be used to explore the mechanism of sulfate reduction coupled to AOM, and below we discuss two important observations using these isotopes: (i) the sulfur and oxygen isotope fractionations and their linear ratio within methane seeps with high rates of sulfate reduction, and (ii) the significantly lower sulfur and oxygen isotope fractionation in the incubation experiments with the addition of hematite.

High sulfate reduction rates were observed in our experiments. Based on the decrease in the concentration of sulfate with time, we calculate that the net sulfate reduction rate was about $1 \cdot 10^{-12} \text{ mol} \cdot \text{cm}^{-3} \cdot \text{s}^{-1}$. This rate of sulfate reduction is similar to natural environments with high sulfate reduction rates such as other methane seeps [e.g., $1 \cdot 10^{-11}$ – $1 \cdot 10^{-14} \text{ mol} \cdot \text{cm}^{-3} \cdot \text{s}^{-1}$ (12)], estuaries [ref. 65, 1 – $7 \cdot 10^{-12} \text{ mol} \cdot \text{cm}^{-3} \cdot \text{s}^{-1}$ (66)], $1 \cdot 10^{-13} \text{ mol} \cdot \text{cm}^{-3} \cdot \text{s}^{-1}$ (50)], and eutrophic lakes [e.g., up to $1.5 \cdot 10^{-12} \text{ mol} \cdot \text{cm}^{-3} \cdot \text{s}^{-1}$ (67)]. These net sulfate reduction rates are much higher than sulfate reduction rates in nonseep-associated marine sediments [e.g., in the Mediterranean Sea, $7 \cdot 10^{-15} \text{ mol} \cdot \text{cm}^{-3} \cdot \text{s}^{-1}$ (50)].

It has been shown that high sulfur isotope fractionation (up to $\sim 70\text{‰}$) correlates with low sulfate reduction rates (e.g., refs. 39 and 40), which is likely due to the increased reoxidation of intracellular sulfur intermediates and full expression of isotope effects associated with each enzymatic step. Conversely, lower sulfur isotope fractionation has been observed during high rates of bacterial sulfate reduction, which is likely due to higher uni-

directional throughput of sulfur through bacterial cells and less reoxidation of the intracellular intermediates (e.g., refs. 39, 40, 68, and 69). Oxygen isotopes in sulfate are particularly sensitive to changes in the reoxidation of sulfur intermediates because of their tendency to exchange oxygen atoms with water within the bacterial cells.

Only a few studies have measured both the sulfur and oxygen isotope fractionation during sulfate-driven AOM, predominantly in the environment (12, 55, 56, 70, 71). The overall sulfur isotope fractionation during AOM in seeps has been shown to be lower than the sulfur isotope fractionation of traditional organoclastic bacterial sulfate reduction or sulfate-driven AOM in long, diffusive profiles. For example, Deusner et al. (71) showed recently in slurry experiments with high unlimited methane concentrations (mimicking seeps) sulfur isotope fractionations of around 20–40‰ during sulfate-driven AOM. In this study, with methane seep sediments, we demonstrate a sulfur isotope fractionation between 21‰ (with the labeled methane and hematite addition) and 40‰ (just with labeled methane), and oxygen isotope fractionation approximately one-half the magnitude of the sulfur isotope fractionation in both experiments. These results fit the experimental data of Deusner et al. (71). The increase in DIC concentration and the decrease in sulfate concentration have the stoichiometry expected by AOM (1:–1) and not that of regular (organoclastic) sulfate reduction (2:–1), supporting also the dominance of AOM over oxidation of other organic compounds. However, it seems that organoclastic bacterial sulfate reduction also occurs in our sediments. This is based on the high ^{13}C -DIC values with the addition of glucose. In addition, organoclastic bacterial sulfate reduction is evident in our experiments with the slightly higher sulfur and oxygen isotope composition in the

glucose addition (highest with labeled glucose addition, slightly lower with labeled methane addition, and much lower with labeled methane and hematite addition; Fig. 3).

The slope in a cross plot of $\delta^{18}\text{O}_{\text{SO}_4}$ vs. $\delta^{34}\text{S}_{\text{SO}_4}$ can be used also to elucidate different types of sulfate reduction (42, 43, 49, 50). Inherent in the interpretation of this slope is how oxygen isotopes in sulfate behave during sulfate reduction, whether only equilibrium oxygen isotope fractionation between sulfur intermediates and water is considered important or whether kinetic oxygen isotope effects at each step are also considered (42, 43, 50, 51). Consideration of both equilibrium and kinetic oxygen isotope effects during sulfate reduction suggests that a larger increase in sulfur and oxygen isotope fractionation correlates with more reoxidation of sulfur intermediates. If the equilibrium oxygen isotope effect dominates, then a linear correlation between $\delta^{18}\text{O}_{\text{SO}_4}$ vs. $\delta^{34}\text{S}_{\text{SO}_4}$ is explained as the tangent of a concave curve, where the curve asymptotically approaches to complete equilibrium between sulfur intermediates and ambient water. If kinetic oxygen isotope effects dominate, then high rates of sulfate reduction with less back reaction of sulfur intermediates lead directly to a linear relationship with low slope (Fig. 4, trend A). In this latter model, lower rates of sulfate reduction with more back reaction of sulfur intermediates lead to the apparent linear phase (higher slope) and asymptotic equilibrium for $\delta^{18}\text{O}_{\text{SO}_4}$ value typical to sulfite exchange with water and oxidation (Fig. 4, trend B).

In our seep experiment incubations, a cross plot of $\delta^{18}\text{O}_{\text{SO}_4}$ vs. $\delta^{34}\text{S}_{\text{SO}_4}$, with and without hematite addition, reveals that the data fall on a line with slope of 0.50 ($r^2 = 0.99$) (Fig. 5). If we take this slope as a strict indication of the mechanism of bacterial sulfate reduction, our methane seep sediments are dominated by both organoclastic sulfate reduction and sulfate-driven AOM with a predominance of sulfate-driven AOM: according to Antler et al. (56), the oxygen and sulfur isotopes in the residual sulfate in the pore fluids are linearly correlated during intensive sulfate-driven AOM with slope of ~ 0.4 , whereas during organoclastic bacterial sulfate reduction, the isotopes evolve in a concaved relationship with apparent linear stage with a slope greater than 0.7.

Addition of hematite to the slurries led to significant microbial iron reduction, stimulated sulfate-driven AOM, and lowered the magnitude of the isotope fractionation of both sulfur and oxygen isotopes in sulfate by about 50% (Fig. 3). These results indicate clearly the involvement of iron oxides during sulfate reduction in seeps. The fact that all experimental setups, with and without

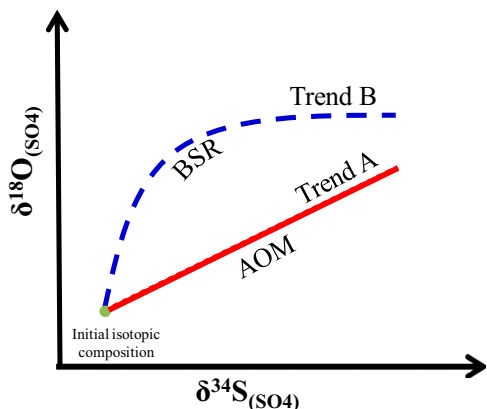


Fig. 4. Typical isotope ratio trends of $\delta^{18}\text{O}_{\text{SO}_4}$ vs. $\delta^{34}\text{S}_{\text{SO}_4}$ in natural environments (modified with permission from ref. 50). High rates of sulfate reduction with less back reaction of sulfur intermediates lead directly to a linear relationship with low slope (trend A), whereas lower rates of sulfate reduction with more back reaction of sulfur intermediates lead to the apparent linear phase (higher slope) and asymptotic equilibrium for $\delta^{18}\text{O}_{\text{SO}_4}$ value typical to sulfite exchange with water and oxidation (trend B).

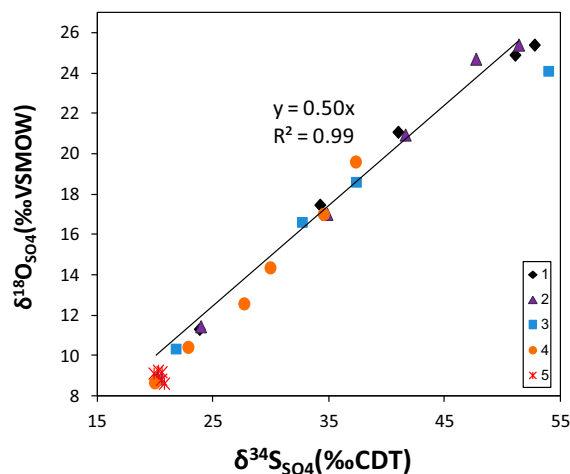


Fig. 5. The ratio between $\delta^{18}\text{O}_{\text{SO}_4}$ and $\delta^{34}\text{S}_{\text{SO}_4}$ in the methane seep sediments of this study along the experiment. The numbers in the legend refer to the different treatments (Table S1).

hematite addition, fall on the same line in a plot of $\delta^{18}\text{O}_{\text{SO}_4}$ vs. $\delta^{34}\text{S}_{\text{SO}_4}$ means that the same mechanism for sulfate reduction existed in all of them. This suggests that the relative forward and backward fluxes within the cells of the microbial communities were the same in all experiments, despite changes in the environmental conditions imposed, including the addition of different carbon sources (glucose and methane) and the addition of hematite. The only difference seems to be the significant 50% smaller overall expressed sulfur and oxygen isotopic fractionation with the addition of hematite (Fig. 3), although the two isotopes evolve relative to one another in a similar manner (Fig. 5). The fact that the slope does not change implies that the addition of hematite stimulates the natural process that was already occurring in the sediment. These results, together with the increase in ^{13}C -labeled DIC in the hematite experiments, indicate that the reduction of natural iron oxides has a role during sulfate-driven AOM. The addition of hematite in our experiments enhanced natural sulfate reduction and intermediate valence state sulfur recycling, thus increasing the gross rates of sulfate reduction and only impacting slightly the overall net sulfate reduction (with the hematite treatment), and lowering the sulfur and oxygen isotope fractionation. The presence of highly reactive iron oxides in the natural sediments was checked using diluted ascorbic acid [with the same procedure of Sivan et al. (22)] and indeed high levels of reactive iron oxides were found in these seeps ($\sim 0.2\%$).

It can be seen that the use of the sulfur and oxygen isotopes in sulfate narrows the initial two options regarding the involvement of iron in the anaerobic oxidation of methane. The first option, that of direct iron-driven AOM, would compete with sulfate-driven AOM and thus would cause a decrease in sulfate reduction rates—here, no decrease was observed in the rate of sulfate removal over time. In addition, a decrease in sulfate reduction rates should lead to an increase in the sulfur and oxygen isotope fractionation during sulfate reduction, where we observe a decrease. The second option, iron stimulation of sulfate-driven AOM, is consistent with all our geochemical measurements; it would increase the rates of sulfate-driven AOM and the recycling of sulfate and would result in a corresponding decrease in the sulfur and oxygen isotope fractionation. Our observations show that iron oxides can stimulate sulfate reduction significantly and, in the case of sulfate-coupled AOM, can stimulate methanotrophy.

In the environment, iron as a key nutrient limits sulfate reduction and may impact the flow of sulfur through the microbial community and therefore the expressed isotope fractionation [e.g., Sim et al.

(72)]. In our experiments amended with high levels of hematite, another plausible explanation is that the redox reaction of oxidized iron with sulfide produced during sulfate-driven AOM or/and precipitation of iron sulfide minerals accelerates sulfate-driven AOM. This occurs by creating more thermodynamically favorable conditions through the removal of the end products, along with the reduction of hematite and other iron oxide compounds (73). It is also possible that iron oxides are recycled and used again by reduction and then reoxidation.

Redox coupling between sulfur and iron resulting in the recycling of sulfur has been previously demonstrated. For example, microbial studies in terrestrial environments illustrated that ferrihydrite can be reduced to ferrous iron through sulfur cycling with intermediate sulfur compounds like thiosulfate and elemental sulfur as the primary reductant (74, 75). These authors also suggested that extremely insoluble iron minerals at ocean Eh-pH could be reduced through similar electron shuttling by intermediate valence state sulfur species. As mentioned above, Holmkvist et al. (64) also showed redox reactions between iron oxides and sulfide (FeS or pyrite) greatly increased sulfate recycling.

It is difficult at this stage to determine the specific pathway of sulfate reduction in the methane seep sediments observed in our study. This mechanism must explain both rapid rates of sulfate reduction, some recycling of sulfur intermediates, and a linear relationship between sulfur and oxygen isotopes. The most reasonable explanation is to keep the “traditional” sulfate reduction mechanism in the linear, more kinetically driven, stage (trend A in Fig. 4) with both sulfur and oxygen increasing as in a Rayleigh-style distillation and recycling by iron of up to 40% [shown by Antler et al. (50) to be the maximum possible recycling that keeps a linear curve]. Another possibility is that our results complete the AOM mechanism recently shown by Milucka et al. (27). In this alternative AOM mechanism, sulfur disproportionating bacteria simultaneously oxidize and reduce zero valence sulfur intermediates to sulfate and sulfide, respectively, in a ratio of 1:7. This mechanism can be completed and the fate of sulfide altered by adding iron, where the presence of iron oxides would help oxidize sulfide to elemental sulfur and polysulfides and then these intermediates would subsequently disproportionate to sulfate and sulfide, as shown by Holmkvist et al. (64). Addition of hematite would increase this recycling without changing the mechanism, thus lowering the expressed sulfur and oxygen isotope fractionation without significantly increasing the net rate of sulfate reduction. It is not clear yet, however, how the sulfur and the oxygen isotopes increase in the same ratio (of ~ 0.5) in this mechanism. One option is that the linear curve between these isotopes represents a mixing line between the residual sulfate from the ANME reduction and the produced sulfate from the disproportionation, which is always isotopically lighter than the residual sulfate pool. The problem would then be to explain the small sulfur and oxygen isotope fractionation during disproportionation, and the constant relative values, although if this end member is small then our results remain valid.

Conclusions

In this study, we documented the coexistence of sulfate reduction, iron reduction, AOM, and methanogenesis in marine seep sediments. This emphasizes that the traditional redox order of bacterial respiration is highly simplified, where, in sediments such as these seeps, all of these processes can occur together with complex couplings between them. The links between these processes were explored, and it was shown that iron reduction is involved in sulfate-driven AOM in seep sediments, stimulating the rate of this microbial process. Our results suggest that, beyond the functions of iron as nutrient, the presence of iron oxides stimulate sulfate-driven AOM to a greater extent than in sediments with low concentrations of iron oxides. We demonstrate also that sulfate reduction in seeps differs from sulfate reduction in diffusive profiles in and above the

sulfate–methane transition zone. This is consistent with recent sulfur isotope fractionation in sulfate recorded from other seep sites under high methane partial pressures (71).

Materials and Methods

Experimental Design. Samples for this study were collected from an area of active methane seepage at Hydrate Ridge South (44° 34.09N; 125° 9.14; water depth, 774 m), 100 km offshore of Oregon, using the manned submersible *Alvin* during R/V *Atlantis* cruise AT 15–68 on August 1, 2010. Microcosm incubation experiments were performed with seep sediments collected beneath a sulfide-oxidizing microbial mat by push coring (AD4629 PC-9; #3443) (Fig. S1). The push core was processed shipboard according to Orphan et al. (24) into 3-cm intervals and sealed in Mylar bags flushed with N₂ gas at 4 °C before microcosm setup. Slurries using sediment from the 9- to 12-cm depth horizon were homogenized in an anaerobic chamber using N₂ purged artificial filtered seawater (final ratio of 1:7 of sediment to seawater). Ten sterile (autoclaved) serum bottles (120-mL volume) were each filled with 50 mL of slurry, and 0.1 g of fine grain hematite was added to four bottles (#4–5) for final concentrations of ferric iron of 12.5 mM. The bottles were sealed then with butyl rubber stoppers. All bottles were then purged twice (5 min each time) with N₂/CO₂ (80/20) and the biological activity was inhibited in two bottles by autoclaving (#5). One hundred microliters of carbon-13 label for methane was injected into eight bottles (#2–5) for final concentration of ~ 5 μ M in the slurry and 150 μ M in the headspace, and 50 μ L of carbon-13 glucose was injected to six bottles (#1, 2, 5) for final concentration of 50 μ M in the slurry. The list of bottles and treatments are described in Table S1. The incubations were maintained in dark at 10–14 °C and sampled periodically over 6 mo.

Analytical Methods. One milliliter of headspace sample was taken for methane analysis from each crimped vial with a gas-tight pressure lock after the bottle was shaken vigorously. Methane concentrations were measured by a gas chromatograph equipped with a flame ionization detector with error of 3%. Three milliliters of the slurry solution were filtered through a 0.45 μ m filter and sampled for ferrous iron concentrations (1 mL), the concentration of DIC, and its carbon isotope composition ($\delta^{13}\text{C}_{\text{DIC}}$; 1 mL) and sulfate concentrations and sulfur and oxygen isotopic compositions ($\delta^{34}\text{S}_{\text{SO}_4}$, $\delta^{18}\text{O}_{\text{SO}_4}$; 1 mL). Ferrous iron was fixed immediately using the Ferrozine method (76), and the absorbance at 562 nm was measured on a spectrophotometer with precision of less than 7 μ M between duplicates. $\delta^{13}\text{C}_{\text{DIC}}$ was measured by a Gas Source Isotopic Ratio Mass Spectrometer (GS-IRMS Thermo; Delta V advantage; Ben Gurion University) through a Gas Bench II interface with error of 0.1‰. The values are reported vs. the Vienna Pee Dee Belemnite standard. DIC concentrations were measured also on the IRMS according to the peak height and calibration curve with precision of 0.2 mM between duplicates. The sample for sulfate concentrations was purged with N₂ for at least 30 min to remove the sulfide. Sulfate concentrations were measured by HPLC (Dionex DX500; Ben Gurion University) with an error of 3% between duplicates. For sulfur and oxygen isotopes in the sulfate, barite (BaSO₄) was precipitated by adding BaCl₂ as described by Antler et al. (50). The barite was pyrolyzed at 1,450 °C in a temperature conversion element analyzer for $\delta^{18}\text{O}_{\text{SO}_4}$ analysis, and the resulting carbon monoxide (CO) was measured by continuous helium flow on a GS-IRMS (Thermo Finnegan Delta V Plus; Godwin Laboratory, University of Cambridge). For the $\delta^{34}\text{S}_{\text{SO}_4}$ analysis, the barite was combusted at 1,030 °C in a flash element analyzer, and the resulting sulfur dioxide (SO₂) was measured by continuous helium flow on a GS-IRMS (Thermo Finnegan Delta V Plus; Godwin Laboratory, University of Cambridge). Samples for $\delta^{18}\text{O}_{\text{SO}_4}$ were run in replicates ($n = 3$ –5) and the SD of these replicate analyses was used as the error ($\sim 0.3\%$ 1 σ). The error for $\delta^{34}\text{S}_{\text{SO}_4}$ was determined using the SD of the standard NBS 127 at the beginning and the end of each run ($\sim 0.3\%$ 1 σ). Samples for both $\delta^{18}\text{O}_{\text{SO}_4}$ and $\delta^{34}\text{S}_{\text{SO}_4}$ were corrected to NBS 127 ($\delta^{18}\text{O}_{\text{SO}_4}$ of 8.6‰ and $\delta^{34}\text{S}_{\text{SO}_4}$ of 20.3‰). $\delta^{34}\text{S}_{\text{SO}_4}$ is reported vs. Vienna Canyon Diablo troilite and $\delta^{18}\text{O}_{\text{SO}_4}$ vs. Vienna standard mean ocean water. Full description of this method is described by Antler et al. (50).

ACKNOWLEDGMENTS. We thank Stephanie Cannon for the help in the laboratory, George Rossman for the hematite powder, and Jiwchar Ganor and his laboratory members for the help with the sulfate measurements. Thanks to Matthias Kellermann and Itay Bar-Or for the help and fruitful discussions. This research was supported by Israel Science Foundation Grant 643/12 (to O.S.), Department of Energy Biological Environmental Research Grant DE-SC0004949, and Gordon and Betty Moore Foundation Marine Microbiology Initiative Grant 3306 (to V.J.O.). Funding for sample collection was provided by National Science Foundation Biological Oceanography Grant 0825791.

1. Froelich PN, et al. (1979) Early oxidation of organic matter in pelagic sediments of the eastern equatorial Atlantic: Suboxic diagenesis. *Geochim Cosmochim Acta* 43:1075–1090.
2. Kasten S, Jørgensen BB (2000) Sulfate reduction in marine sediments. *Marine Geochemistry*, eds Schulz HD, Zabel M (Springer, Berlin), pp 263–281.
3. Whiticar MJ, Faber E, Schoell M (1986) Biogenic methane formation in marine and freshwater environments: CO₂ reduction vs. acetate fermentation-isotope evidence. *Geochim Cosmochim Acta* 50:693–709.
4. Chistoserdova L, Vorholt JA, Lidstrom ME (2005) A genomic view of methane oxidation by aerobic bacteria and anaerobic archaea. *Genome Biol* 6(2):208.
5. Bastviken DL, Cole JJ, Pace ML, van de Bogert MC (2008) Fates of methane from different lake habitats: Connecting whole-lake budgets and CH₄ emissions. *J Geophys Res Biogeosci* 113:G02024.
6. Martens CS, Berner RA (1977) Interstitial water chemistry of anoxic Long Island Sound sediments. 1. *Limnol Oceanogr* 22:10–25.
7. Hoehler TM, Alperin MJ, Albert DB, Martens CS (1994) Field and laboratory studies of methane oxidation in an anoxic marine sediment: Evidence for a methanogen-sulfate reducer consortium. *Global Biogeochem Cycles* 8(4):451–463.
8. Valentine DL (2002) Biogeochemistry and microbial ecology of methane oxidation in anoxic environments: A review. *Antonie van Leeuwenhoek* 81(1–4):271–282.
9. Borowski WS, Paull CK, Ussler W (1996) Marine pore fluid sulfate profiles indicate in situ methane flux from underlying gas hydrate. *Geology* 24:655–658.
10. Niewöhner C, Hensen C, Kasten S, Zabel M, Schulz H (1998) Deep sulfate reduction completely mediated by anaerobic methane oxidation in sediments of the upwelling area off Namibia. *Geochim Cosmochim Acta* 62(3):455–464.
11. Boetius A, et al. (2000) A marine microbial consortium apparently mediating anaerobic oxidation of methane. *Nature* 407(6804):623–626.
12. Aharon P, Fu B (2000) Microbial sulfate reduction rates and sulfur and oxygen isotope fractionations at oil and gas seeps in deepwater Gulf of Mexico. *Geochim Cosmochim Acta* 64(2):233–246.
13. Sivan O, Schrag DP, Murray RW (2007) Rates of methanogenesis and methanotrophy in deep-sea sediments. *Geobiology* 5:141–151.
14. Zehnder AJB, Brock TD (1980) Anaerobic methane oxidation: Occurrence and ecology. *Appl Environ Microbiol* 39(1):194–204.
15. Beal EJ, House CH, Orphan VJ (2009) Manganese- and iron-dependent marine methane oxidation. *Science* 325(5937):184–187.
16. Riedinger N, et al. (2014) An inorganic geochemical argument for coupled anaerobic oxidation of methane and iron reduction in marine sediments. *Geobiology* 12(2):172–181.
17. Raghoebaring AA, et al. (2006) A microbial consortium couples anaerobic methane oxidation to denitrification. *Nature* 440(7086):918–921.
18. Ettwig KF, van Alen T, van de Pas-Schoonen KT, Jetten MS, Strous M (2009) Enrichment and molecular detection of denitrifying methanotrophic bacteria of the NC10 phylum. *Appl Environ Microbiol* 75(11):3656–3662.
19. Ettwig KF, et al. (2010) Nitrite-driven anaerobic methane oxidation by oxygenic bacteria. *Nature* 464(7288):543–548.
20. Haroon MF, et al. (2013) Anaerobic oxidation of methane coupled to nitrate reduction in a novel archaeal lineage. *Nature* 500(7464):567–570.
21. Norði KA, Thamdrup B (2014) Nitrate-dependent anaerobic methane oxidation in a freshwater sediment. *Geochim Cosmochim Acta* 132:141–150.
22. Sivan O, et al. (2011) Geochemical evidence for iron-mediated anaerobic oxidation of methane. *Limnol Oceanogr* 56:1536–1544.
23. Norði KA, Thamdrup B, Schubert CJ (2013) Anaerobic oxidation of methane in an iron-rich Danish freshwater lake sediment. *Limnol Oceanogr* 58(2):546–554.
24. Orphan VJ, House CH, Hinrichs KU, McKeegan KD, DeLong EF (2001) Methane-consuming archaea revealed by directly coupled isotopic and phylogenetic analysis. *Science* 293(5529):484–487.
25. Thauer RK, Shima S (2006) Biogeochemistry: Methane and microbes. *Nature* 440(7086):878–879.
26. Basen M, et al. (2011) Bacterial enzymes for dissimilatory sulfate reduction in a marine microbial mat (Black Sea) mediating anaerobic oxidation of methane. *Environ Microbiol* 13(5):1370–1379.
27. Milucka J, et al. (2012) Zero-valent sulphur is a key intermediate in marine methane oxidation. *Nature* 491(7425):541–546.
28. Whiticar MJ (1999) Carbon and hydrogen isotope systematics of bacterial formation and oxidation of methane. *Chem Geol* 161:291–314.
29. Borowski WS, Gagatay N, Ternois Y, Paull CK (2000) Data report: Carbon isotopic composition of dissolved CO₂, CO₂ gas, and methane, Blake-Bahama Ridge and northeast Bermuda Rise, ODP Leg 172. *Proc Ocean Drill Program Sci Results* 172:1–16.
30. Alperin MJ, Reeburgh WS, Whiticar MJ (1988) Carbon and hydrogen isotope fractionation resulting from anaerobic methane oxidation. *Global Biogeochem Cycles* 2(3):279–288.
31. Martens CS, Albert DB, Alperin MJ (1999) Stable isotope tracing of anaerobic methane oxidation in the gassy sediments of Eckernförde Bay, German Baltic Sea. *Am J Sci* 299(7–9):589–610.
32. Habicht KS, Canfield DE (1997) Sulfur isotope fractionation during bacterial sulfate reduction in organic-rich sediments. *Geochim Cosmochim Acta* 61(24):5351–5361.
33. Wortmann UG, Bernasconi SM, Böttcher ME (2001) Hypersulfidic deep biosphere indicates extreme sulfur isotope fractionation during single-step microbial sulfate reduction. *Geology* 29:647–650.
34. Brunner B, Bernasconi SM (2005) A revised isotope fractionation model for dissimilatory sulfate reduction in sulfate. *Geochim Cosmochim Acta* 69(20):4759–4771.
35. Sim MS, Bosak T, Ono S (2011) Large sulfur isotope fractionation does not require disproportionation. *Science* 333(6038):74–77.
36. Rees CE (1973) A steady-state model for sulphur isotope fractionation in bacterial reduction processes. *Geochim Cosmochim Acta* 37(5):1141–1162.
37. Canfield DE (2001) Biogeochemistry of sulfur isotopes. *Reviews in Mineralogy and Geochemistry* 43, eds Valley JW, Cole DR (Mineralogical Society of America, Blacksburg, VA), pp 607–636.
38. Farquhar J, et al. (2003) Multiple sulphur isotopic interpretations of biosynthetic pathways: Implications for biological signatures in the sulphur isotope record. *Geobiology* 1:27–36.
39. Canfield DE, Olesen CA, Cox RP (2006) Temperature and its control of isotope fractionation by a sulfate-reducing bacterium. *Geochim Cosmochim Acta* 70:548–561.
40. Sim MS, Ono S, Donovan K, Templar SP, Bosak T (2011) Effect of electron donors on the fractionation of sulfur isotopes by a marine *Desulfovibrio* sp. *Geochim Cosmochim Acta* 75:4244–4259.
41. Fritz P, Basharmal GM, Drimmie RJ, Ibsen J, Qureshi RM (1989) Oxygen isotope exchange between sulfate and water during bacterial reduction of sulfate. *Chem Geol* 79:99–105.
42. Brunner B, Bernasconi SM, Kleikemper J, Schroth MJ (2005) A model for oxygen and sulfur isotope fractionation in sulfate during bacterial sulfate reduction processes. *Geochim Cosmochim Acta* 69:4773–4785.
43. Brunner B, et al. (2012) The reversibility of dissimilatory sulphate reduction and the cell-intrafractionation of sulphite to sulphide: Insights from the oxygen isotope composition of sulphate. *Isotopes Environ Health Stud* 48(1):33–54.
44. Mangalo M, Meckenstock RU, Stichler W, Einsiedl F (2007) Stable isotope fractionation during bacterial sulfate reduction is controlled by reoxidation of intermediates. *Geochim Cosmochim Acta* 71:4161–4171.
45. Mangalo M, Einsiedl F, Meckenstock RU, Stichler W (2008) Influence of the enzyme dissimilatory sulfite reductase on stable isotope fractionation during sulfate reduction. *Geochim Cosmochim Acta* 71:4161–4171.
46. Eckert T, Brunner B, Edwards EA, Wortmann UG (2011) Microbially mediated re-oxidation of sulfide during dissimilatory sulfate reduction by *Desulfobacter latus*. *Geochim Cosmochim Acta* 75:3469–3485.
47. Holler T, et al. (2011) Carbon and sulfur back flux during anaerobic microbial oxidation of methane and coupled sulfate reduction. *Proc Natl Acad Sci USA* 108(52):E1484–E1490.
48. Turchyn AV, Sivan O, Schrag D (2006) Oxygen isotopic composition of sulfate in deep sea pore fluid: Evidence for rapid sulfur cycling. *Geobiology* 4:191–201.
49. Wortmann UG, et al. (2007) Oxygen isotope biogeochemistry of pore water sulfate in the deep biosphere: Dominance of isotope exchange reactions with ambient water during microbial sulfate reduction (ODP Site 1130). *Geochim Cosmochim Acta* 71(17):4221–4232.
50. Antler G, Turchyn AV, Rennie V, Herut B, Sivan O (2013) Coupled sulfur and oxygen isotope insight into bacterial sulfate reduction in the natural environment. *Geochim Cosmochim Acta* 118:98–117.
51. Wankel SD, Bradley AS, Eldridge DL, Johnston DT (2013) Determination and application of the equilibrium oxygen isotope effect between water and sulfite. *Geochim Cosmochim Acta* 125:694–711.
52. Turchyn AV, et al. (2010) Kinetic oxygen isotope effects during dissimilatory sulfate reduction: A combined theoretical and experimental approach. *Geochim Cosmochim Acta* 74:2011–2024.
53. Böttcher ME, Brumsack HJ, de Lange GJ (1998) Sulfate reduction and related stable isotope (³⁴S, ¹⁸O) variations in interstitial waters from the eastern Mediterranean. *Proc Ocean Drill Program Sci Results* 160:365–373.
54. Böttcher ME, Bernasconi SM, Brumsack HJ (1999) Carbon, sulfur, and oxygen isotope geochemistry of interstitial waters from the western Mediterranean. *Proc Ocean Drill Program Sci Results* 161:413–421.
55. Aharon P, Fu B (2003) Sulfur and oxygen isotopes of coeval sulfate-sulfide in pore fluids of cold seep sediments with sharp redox gradients. *Chem Geol* 195(1):201–218.
56. Antler G, et al. (2014) Sulfur and oxygen isotope tracing of sulfate driven anaerobic methane oxidation in estuarine sediments. *Estuar Coast Shelf Sci* 142:4–11.
57. House CH, et al. (2009) Extensive carbon isotopic heterogeneity among methane seep microbiota. *Environ Microbiol* 11(9):2207–2215.
58. Postma D (1993) The reactivity of iron oxides in sediments: A kinetic approach. *Geochim Cosmochim Acta* 57:5027–5034.
59. Girguis PR, Orphan VJ, Hallam SJ, DeLong EF (2003) Growth and methane oxidation rates of anaerobic methanotrophic archaea in a continuous-flow bioreactor. *Appl Environ Microbiol* 69(9):5472–5482.
60. Nauhaus K, Treude T, Boetius A, Krüger M (2005) Environmental regulation of the anaerobic oxidation of methane: A comparison of ANME-1 and ANME-1 communities. *Environ Microbiol* 7(1):98–106.
61. Orphan VJ, Turk KA, Green AM, House CH (2009) Patterns of ¹⁵N assimilation and growth of methanotrophic ANME-2 archaea and sulfate-reducing bacteria within structured syntrophic consortia revealed by FISH-SIMS. *Environ Microbiol* 11(7):1777–1791.
62. Yoshinaga MY, et al. (2014) Carbon isotope equilibration during sulphate-limited anaerobic oxidation of methane. *Nat Geosci* 7:190–194.
63. Ertefai TF, et al. (2010) The biogeochemistry of sorbed methane in marine sediments. *Geochim Cosmochim Acta* 74:6033–6048.
64. Holmkvist L, Ferdelman TG, Jørgensen BB (2011) A cryptic sulfur cycle driven by iron in the methane zone of marine sediment (Aarhus Bay, Denmark). *Geochim Cosmochim Acta* 75:3581–3599.
65. Marvin-DiPasquale MC, Boynton WR, Capone DG (2003) Benthic sulfate reduction along the Chesapeake Bay central channel. II. Temporal controls. *Mar Ecol Prog Ser* 260:55–70.
66. Eliani-Russak E, Herut B, Sivan O (2013) The role of highly stratified nutrient-rich small estuaries as a source of dissolved inorganic nitrogen to coastal seawater, the Qishon (SE Mediterranean) case. *Mar Pollut Bull* 71(1–2):250–258.

67. Adler M, Eckert W, Sivan O (2011) Quantifying rates of methanogenesis and methanotrophy in Lake Kinneret sediments (Israel) using pore-water profiles. *Limnol Oceanogr* 56:1525–1535.
68. Kaplan IR, Rittenberg SC (1964) Microbiological fractionation of sulphur isotopes. *J Gen Microbiol* 34:195–212.
69. Chambers LA, Trudinger PA, Smith JW, Burns MS (1975) Fractionation of sulfur isotopes by continuous cultures of *Desulfovibrio desulfuricans*. *Can J Microbiol* 21(10):1602–1607.
70. Avrahamov N, et al. (2014) Anaerobic oxidation of methane by sulfate in hypersaline groundwater of the Dead Sea aquifer. *Geobiology*, in press.
71. Deusner C, et al. (2014) Sulfur and oxygen isotope fractionation during sulfate reduction coupled to anaerobic oxidation of methane is dependent on methane concentration. *EPSL* 399:61–73.
72. Sim MS, Ono S, Bosak T (2012) Effects of iron and nitrogen limitation on sulfur isotope fractionation during microbial sulfate reduction. *Appl Environ Microbiol* 78(23):8368–8376.
73. Royer RA, Burgos WD, Fisher AS, Unz RF, Dempsey BA (2002) Enhancement of biological reduction of hematite by electron shuttling and Fe(II) complexation. *Environ Sci Technol* 36(9):1939–1946.
74. Straub KL, Schink B (2004) Ferrihydrite-dependent growth of *Sulfurospirillum delleyianum* through electron transfer via sulfur cycling. *Appl Environ Microbiol* 70(10):5744–5749.
75. Straub KL, Schink B (2004) Ferrihydrite reduction by *Geobacter* species is stimulated by secondary bacteria. *Arch Microbiol* 182(2-3):175–181.
76. Stookey LL (1970) Ferrozine- a new spectrophotometric reagent for iron. *Anal Chem* 42:779–781.